Soils and Foundations 2013;53(5):735–745

The Japanese Geotechnical Society

Soils and Foundations

www.sciencedirect.com
journal homepage: www.elsevier.com/locate/sandf

Laboratory measurements of small strain properties of dry sands by bender element

Xiaoqiang Gu[a,*,1], Jun Yang[b,2], Maosong Huang[a,3]

[a]Department of Geotechnical Engineering & Key Laboratory of Geotechnical and Underground Engineering of the Ministry of Education, Tongji University, Shanghai 200092, China

[b]Department of Civil Engineering, The University of Hong Kong, Pokfulam, Hong Kong, China

Received 18 July 2012; received in revised form 17 May 2013; accepted 24 July 2013
Available online 1 October 2013

Abstract

The S-wave and P-wave velocities in dry sands are simultaneously measured by a single pair of bender elements (BE) incorporated into a standard resonant column (RC) apparatus with a torsional shear (TS) function. The small strain properties, including shear modulus G_0, constrained modulus M_0 and Poisson's ratio υ, are determined for specimens at various densities and confining pressures. The results show that the G_0 values obtained from the BE tests agree well with those from RC and TS tests, indicating the reliability of the signal interpretation and the testing system. Furthermore, the G_0 data of the present test series is in good agreement with the data from the literature. The results also show that G_0 increases faster than M_0 as the soil density and the confining pressure increase. In terms of Poisson's ratio, it decreases with an increasing soil density and confining pressure and generally lies in the range of 0.18–0.32 for the tested sands. Empirical equations are established to approximately estimate Poisson's ratio from the measured G_0 or M_0 values.

Keywords: Laboratory test; Bender element; Resonant column; Sand; Wave velocity; Modulus; Poisson's ratio

1. Introduction

It is well recognized that soil behavior is generally nonlinear and plastic in nature. However, at strain levels below 0.001%, the response of soils is usually assumed to be linear and elastic and the corresponding properties are referred to as small strain or elastic properties. The small strain properties of soil play an important role in many geotechnical problems, such as machine foundations, earthquake ground response analyses and liquefaction potential evaluations (e.g., Richart et al. (1970), Andrus and Stokoe II (2000), Yang and Yan (2009)). The small strain properties of soil include shear modulus G_0, Young's modulus E_0, bulk modulus K_0, constrained modulus M_0 and Poisson's ratio υ. For an isotropic continuum, only two parameters are independent. The relation between these parameters can be expressed as follows:

$$G_0 = \frac{E_0}{2(1+\upsilon)} = \frac{3K_0(1-2\upsilon)}{2(1+\upsilon)} = \frac{M_0(1-2\upsilon)}{2(1-\upsilon)} \quad (1)$$

In the laboratory, G_0 and E_0 or G_0 and M_0 are usually measured together to determine the small strain properties (Hardin and

*Corresponding author. Tel.: +86 21 65983980; fax: +86 21 65985210.
E-mail addresses: gxq1981@gmail.com (X. Gu), junyang@hku.hk (J. Yang), mshuang@tongji.edu.cn (M. Huang).
[1]Formerly of The University of Hong Kong.
[2]Tel.: +852 22415273; fax: +852 25595337.
[3]Tel.: +86 21 65983980; fax: +86 21 65985210.
Peer review under responsibility of The Japanese Geotechnical Society.

Production and hosting by Elsevier

0038-0806 © 2013 The Japanese Geotechnical Society. Production and hosting by Elsevier B.V. All rights reserved.
http://dx.doi.org/10.1016/j.sandf.2013.08.011

Richart, 1963; Kokusho, 1980; Nakagawa et al., 1997; Ezaoui and Di Benedetto, 2009; Kumar and Madhusudhan, 2010).

Several techniques have been developed in the geotechnical profession for measuring small strain properties, including resonant columns (Hardin and Richart, 1963; Cascante et al., 1998), piezoelectric transducers (Brignoli et al., 1996; Nakagawa et al., 1997; Lings and Greening, 2001; Kumar and Madhusudhan, 2010; Murillo et al., 2011) and quasi-static loading with high resolution strain measurements (Kokusho, 1980; Hoque and Tatsuoka, 1998; Ezaoui and Di Benedetto, 2009). In resonant columns, G_0 is usually measured by torsional vibrations, while E_0 is obtained from longitudinal vibrations or flexural vibrations at small strain levels. In the quasi-static loading method, the strain is directly measured when the specimen is subjected to a small load increment, and modulus G_0 or E_0 is then determined from the related stress–strain curves. Furthermore, due to the development of piezoelectric transducers, particularly bender elements, both shear waves (S-waves) and primary waves (P-waves) can be easily measured together to evaluate G_0 and M_0, which can be calculated as follows:

$$G_0 = \rho(V_s)^2 \tag{2}$$

$$M_0 = \rho(V_P)^2 \tag{3}$$

where ρ is the density of the soil in the wave propagation, and V_s and V_p are the S-wave and the P-wave velocities in the soil, respectively.

In the past several decades, tremendous studies have been carried out on small strain properties, especially G_0. Both theoretical considerations and experimental results have shown that the small strain modulus of granular soils mainly depends on void ratio e (or soil density) and effective confining pressure σ', and can be expressed by the following general form (Hardin and Richart, 1963):

$$G_0(\text{or } E_0,\ K_0,\ M_0) = AF(e)\left(\frac{\sigma'}{p_a}\right)^n \tag{4}$$

where A is a constant reflecting soil type, grain properties and fabric, p_a is a reference stress (98 kPa in this study), n is the stress exponent reflecting the effect of the confining pressure and $F(e)$ is a void ratio function reflecting the effect of soil density.

Poisson's ratio is frequently adopted in the analysis as one of the two independent parameters in Eq. (1). It is usually assumed to be a constant for a given soil, which means that the void ratio and the confining pressure have identical effects on different moduli based on Eqs. (1) and (4). However, several laboratory tests indicate that Poisson's ratio may depend on e and σ' (Kokusho, 1980; Nakagawa et al., 1997; Kumar and Madhusudhan, 2010; Wichtmann and Triantafyllidis, 2010). Therefore, it is meaningful to investigate the potential difference in the effects of e and σ' on different moduli or the effects of e and σ' on Poisson's ratio in a systematical manner.

In this study, the S-wave and P-wave velocities in three dry sands at different packing densities and effective confining pressures are measured simultaneously by a single pair of bender elements incorporated in a resonant column apparatus with a torsional shear function. Small strain shear modulus G_0 and constrained modulus M_0 as well as Poisson's ratio υ of the soil are evaluated. The effects of the void ratio and the effective confining pressure on G_0, M_0 and υ are quantitatively analyzed. The obtained Poisson's ratios are compared with those of clean sands in the literature, and correlations are established between υ and G_0 or M_0.

2. Test apparatus, material and procedure

2.1. Test apparatus

The bender elements (BE), incorporated in a standard resonant column (RC) apparatus, are used to simultaneously measure the S-wave and P-wave velocities in dry sands. The RC apparatus used in this study is of a bottom-fixed and top-free configuration; it is schematically shown in Fig. 1. It is equipped with an electromagnetic driving head with precision wound coils and internally mounted, counter balanced accelerometers. It can accommodate a soil specimen up to 50 mm in diameter and 100 mm in height, with a cell pressure capacity of 1 MPa. The axial deformation of the specimen is measured by an internal high-resolution LVDT. Furthermore, a slow rate torsional shear (TS) function is also incorporated into this RC.

Fig. 2 schematically shows the bender element testing system. The elements are 11 mm in width and 1.2 mm in thickness, with a protruding depth of 2.0 mm. By modifying the wiring configuration (Lings and Greening, 2001), this single pair of bender elements is able to generate not only S-waves, but also P-waves. The S-wave transmitter or the P-wave receiver is mounted in the top cap, while the S-wave receiver or the P-wave transmitter is mounted in the pedestal. The switch between the S-wave and P-wave tests is automatically done by an external control box, which also plays the role of the transducer power supply and amplification device. Both sinusoidal and square input waveforms at different frequencies can be generated, with a maximum voltage of ± 7 V. The transformation between the digital conversion signal and the analog conversion signal is achieved by a 16-bit high speed data acquisition card installed in the computer. The sampling frequency is 2000 kHz, corresponding to a sampling interval of 0.5 μs.

The system delay is found to be 5.5 μs by the calibration test with element tips in direct contact (Viggiani and Atkinson, 1995; Wang et al., 2007). The calibration test also indicates that the initial polarizations of the input and output signals are the same; this will also be the case in the following if without specification. Special attention should be paid to such an initial polarization relation as it will change in the S-wave test once one element (usually the element on the top cap) rotates 180° to the other. Clearness of this initial polarization relation will benefit the correct determination of the first arrival of the real S-wave, which is usually interfered by the near field component whose initial polarization is opposite to the real S-wave.

2.2. Test material and procedure

Three dry uniform sands, named Toyoura, Fujian and Leighton Buzzard (LB), are used in the test program. Fig. 3 shows their

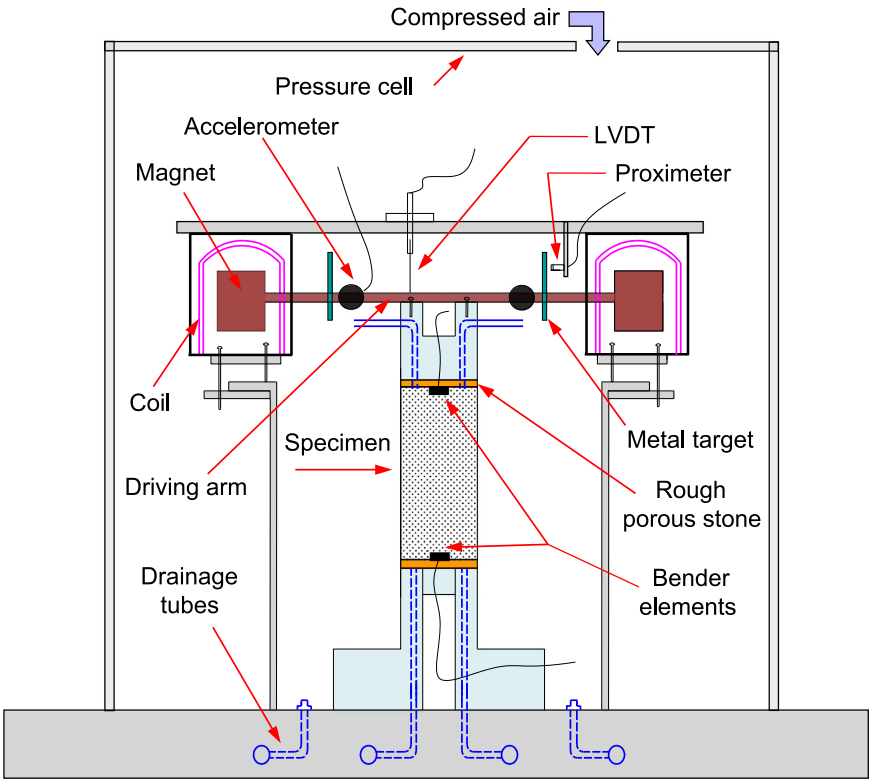

Fig. 1. Schematic illustration of the resonant column apparatus with bender element (not to scale).

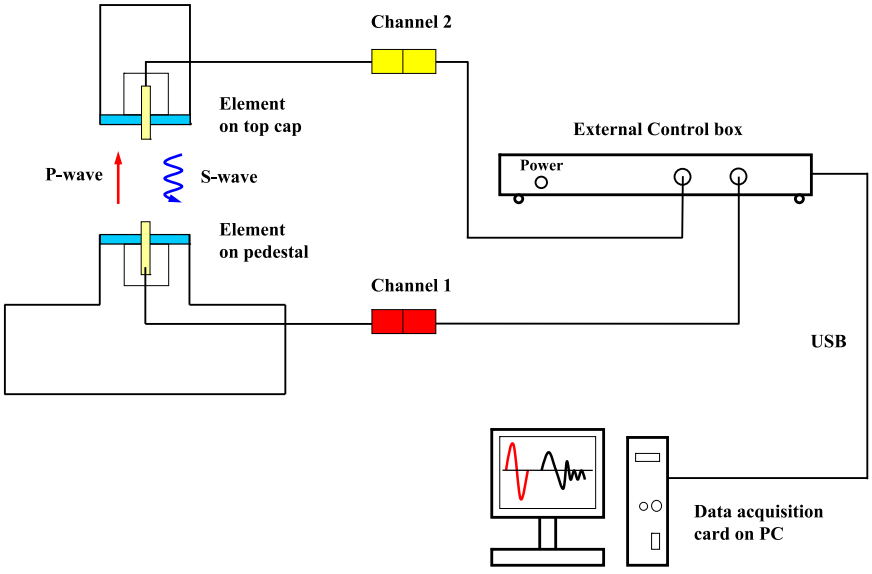

Fig. 2. Schematic illustration of the bender element testing system.

particle size distribution curves together with SEM pictures of their particle shapes. Their main properties are listed in Table 1.

The specimens are prepared in five layers by the dry tamping method. After preparation, a suction of 25 kPa is applied to stabilize the specimens. The dimensions of the specimens are measured accurately and the initial void ratio is determined. The cell pressure is then increased and the suction is decreased simultaneously to keep a constant isotropic effective stress of 25 kPa, which is taken as the initial stress state. Then, the cell pressure is increased in four steps, namely, 50, 100, 200 and 400 kPa (in several tests, the final stress level is 50, 100 or 200 kPa). Note that the axial stress induced by the weights of the top cap and the driving arm with magnets (see Fig. 1) is around 5.4 kPa; and therefore, the stress anisotropy is small. At each stress state, the axial deformation is measured by the LVDT after 15 min of consolidation and the void ratio is updated with an assumption of isotropic deformation. Finally, S-wave and P-wave measurements by bender elements, together with resonant column and

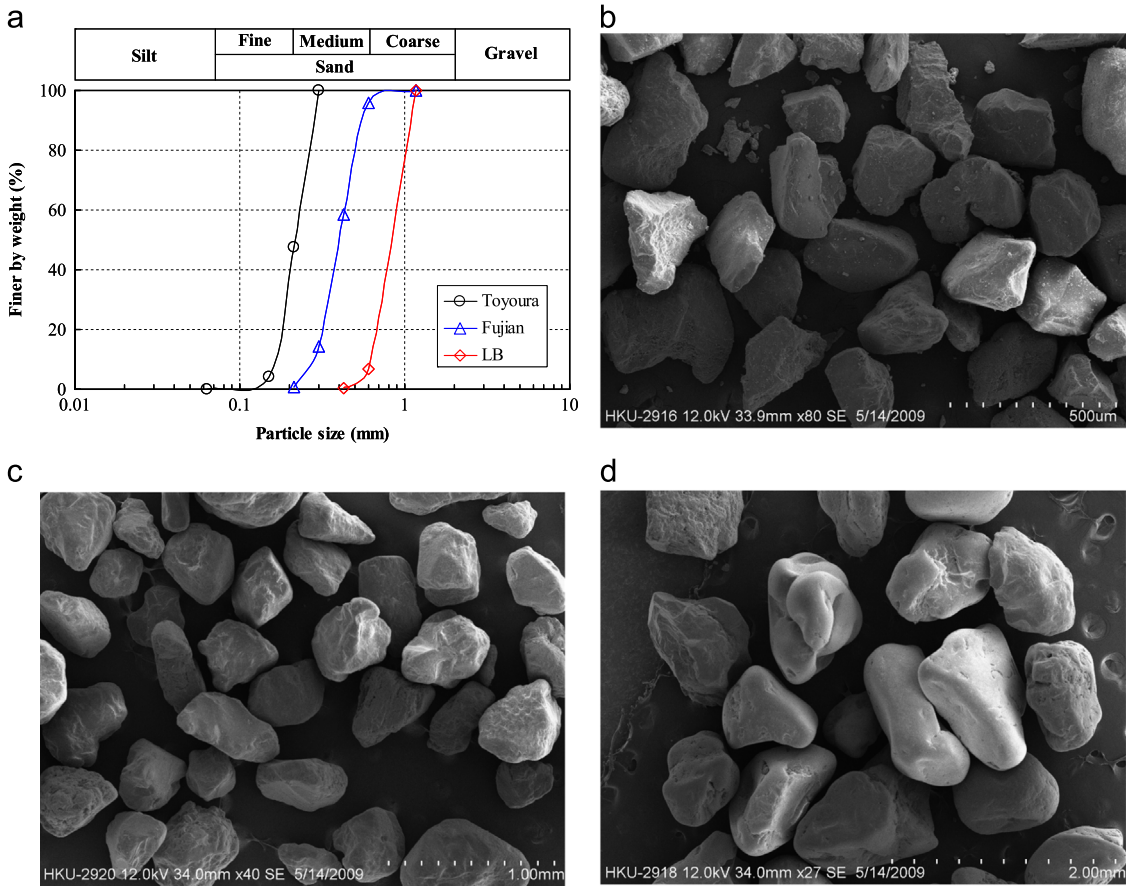

Fig. 3. (a) Particle size distribution curves and SEM pictures of (b) Toyoura, (c) Fujian and (d) LB sands.

Table 1
Main properties of three tested sands.

Sand	G_s	D_{10} (mm)	D_{50} (mm)	D_{60} (mm)	C_u	C_c	e_{max}	e_{min}
Toyoura	2.64	0.166	0.216	0.231	1.392	0.971	0.967	0.633
Fujian	2.65	0.282	0.397	0.432	1.532	0.977	0.879	0.555
LB	2.65	0.620	0.840	0.900	1.452	0.937	0.791	0.523

torsional shear tests at small strain levels, are performed at each specified stress state.

3. Results and discussions

3.1. Signal interpretation

By monitoring the input and output signals in the BE tests, wave velocity V, either V_s or V_p, can be calculated as follows:

$$V = \frac{L_{tt}}{\Delta t} \tag{5}$$

where L_{tt} and Δt are the travel distance and the travel time of the wave, respectively.

It is well agreed that the tip-to-tip distance between the source and the receiver elements can be taken as the travel distance, L_{tt} (Dyvik and Madshus, 1985; Viggiani and Atkinson, 1995; Lee and Santamarina, 2005; Yamashita et al., 2009). However, despite the increasing popularity of the S-wave measurement, signal interpretation and the determination of travel time Δt in the BE tests are still tricky problems involving subjectivity and uncertainty, primarily due to the near field effect and signal distortion (Wang et al., 2007). Compared with the S-waves, the first arrival and the travel time of the P-waves can be easily determined (Brignoli et al., 1996; Leong et al., 2009).

Fig. 4 shows the received P-waves in a dry Toyoura sand specimen by one cycle of sinusoidal input at different frequencies. The specimen is isotropically confined at a pressure of 100 kPa and has a void ratio of 0.798. As seen in Fig. 4, the first arrival of the P-wave is clear at all input frequencies and the travel time can be easily determined to be 225 μs, although the output signal has many cycles and is much more complex than the input signal. Moreover, it is of interest to note that the amplitude of the first arrival is smaller than the succeeding ones.

Compared with the P-waves, the received S-wave signals are much more complicated, as shown in Fig. 5. The downward triangle indicates the P-wave travel time in this specimen. The first part of the received signal is confirmed to be the near field component, as its polarization is opposite to the input, and the corresponding arrival time is near the value of the P-wave propagation, which is in good agreement with the theory (Sanchez-Salinero et al., 1986). Both the theoretical analysis (Sanchez-Salinero et al., 1986) and the experiment (Dyvik and Madshus, 1985) indicate that the polarization of the near field component will also be reversed when the input signal is

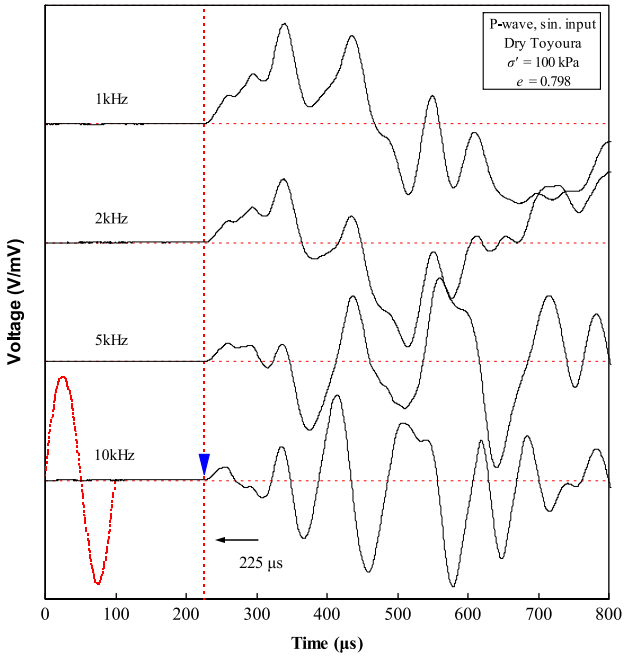

Fig. 4. Received P-wave signals in dry Toyoura sand.

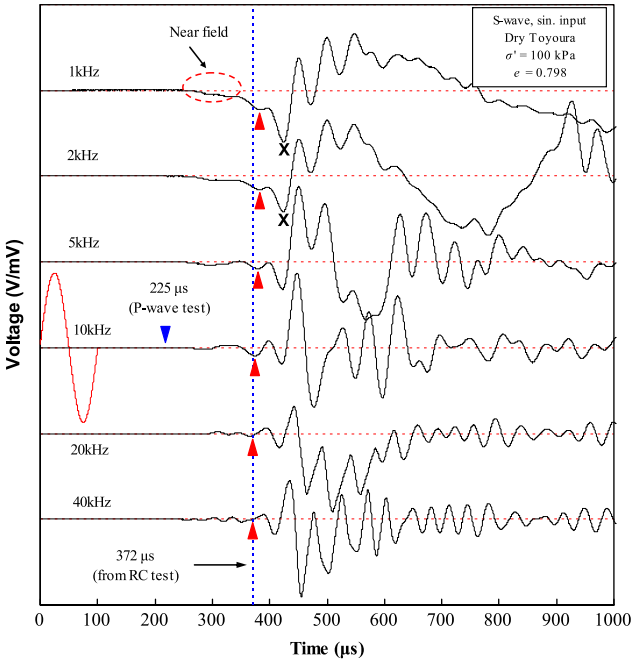

Fig. 5. Received S-wave signals in dry Toyoura sand.

reversed. Therefore, the signal interpretation cannot be improved by reversing the input signal (Viggiani and Atkinson, 1995).

By analyzing the characteristics of the output signals and taking the RC test results at a shear strain level of 6.9×10^{-6} as a reference (indicated by the dashed line in Fig. 5), the first arrival of the S-wave is indicated by the upward triangle in Fig. 5. Bonal et al. (2012) indicated that the results using this characteristic point are consistent with those from the advanced wavelet analysis. Similar to the P-wave, the amplitude of the first arrival of the S-wave is much smaller than the succeeding ones. Thus, care should be taken in locating the first arrival, especially at low frequencies, because the first arrival of the S-wave can be masked by the near field component (e.g., the point indicated by "x" may easily be selected as the first arrival of the S-wave). As seen in Fig. 5, the bump is clearest in the output signal with an input of 10 kHz. For simplicity, therefore, the travel time of the S-wave at 10 kHz is taken as the travel time of the specimen in the following.

To evaluate the reliability of the signal interpretation and the testing system, the G_0 values for Toyoura sand from the BE tests are compared with those from the RC and TS tests on the same specimens and with the data collected from the literature, as shown in Fig. 6. Note that the strain amplitudes in these RC and TS tests are less than 8×10^{-6}. The G_0 values from the BE tests are slightly higher than those from the RC and TS tests. The possible reasons for this difference may be that (a) the strain level in the BE tests is somehow lower than that in the RC and TS tests and (b) the RC and TS tests measure the overall stiffness of the specimen, whereas the BE test measures the local stiffness of the wave travel path, which tends to be stiffer than the whole specimen. Generally, the G_0 values for Toyoura sand from the BE, RC and TS tests in this study agree well with the values in the literature. The received P-wave and S-wave signals in the three sands are compared in Fig. 7. It is clear that the characteristics of the received wave signals are similar, although the wave travel times are different. Similar to Toyoura sand, the G_0 values from the BE tests also agree well with those from the RC and TS tests for Fujian and LB sands. The above results convincingly confirm the reliability of the signal interpretation and the BE testing system.

3.2. G_0 and M_0

Fig. 8 shows the variations in elastic modulus with the void ratio for the three sands at a confining pressure of 100 kPa. Evidently, the elastic modulus decreases as the void ratio increases (or the density decreases), as expected. To quantitatively study the potential difference in the effect of the void ratio on G_0 and M_0, a void ratio function $F(e)=e^{-x}$ (Lo Presti et al., 1997) is used to fit the data at each confining pressure; the best-fit parameters are listed in Table 2. It is of interest to note that at a given confining pressure, void ratio exponent x for G_0 is always larger than that for M_0. This indicates that the effect of the void ratio on G_0 is more profound than that on M_0. Moreover, the x value for G_0 decreases as the confining pressure increases, indicating that the effect of the void ratio on G_0 is more significant at low confining pressures. On the other hand, such a trend is not obvious for M_0.

Taking the average of the x values at different confining pressures as the one in the void ratio function, the G_0 and M_0 values are fitted by Eq. (4) and shown in Fig. 9. For each of the three sands, both the normalized G_0 and M_0 are successfully predicted by a power law to the confining pressure. The average stress exponents n for G_0 are 0.41, 0.45 and 0.35 for Toyoura, Fujian and LB sands, respectively. Meanwhile, the average stress exponents n for M_0 are 0.36, 0.41 and 0.32 for Toyoura, Fujian and LB sands, respectively. Generally, these stress exponents are larger than the value of 1/3 of those predicted by the classical Hertz–Mindlin contact law (Duffy and Mindlin, 1957). Studies on quartz sand also showed that n values for G_0 and M_0 increase

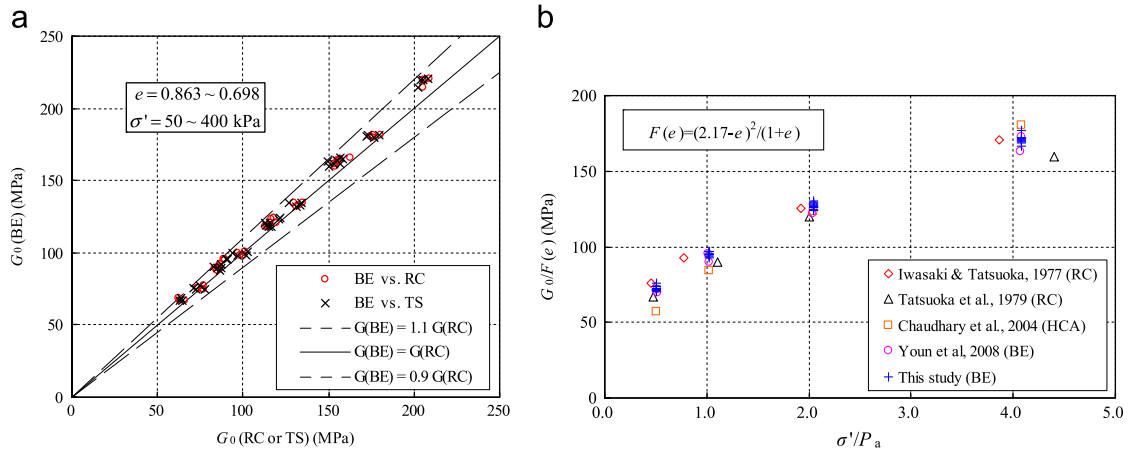

Fig. 6. Comparison of G_0 of Toyoura sand obtained by BE with (a) RC and (b) data in literature (Chaudhary et al., 2003; Tatsuoka et al., 1979; Youn et al., 2008).

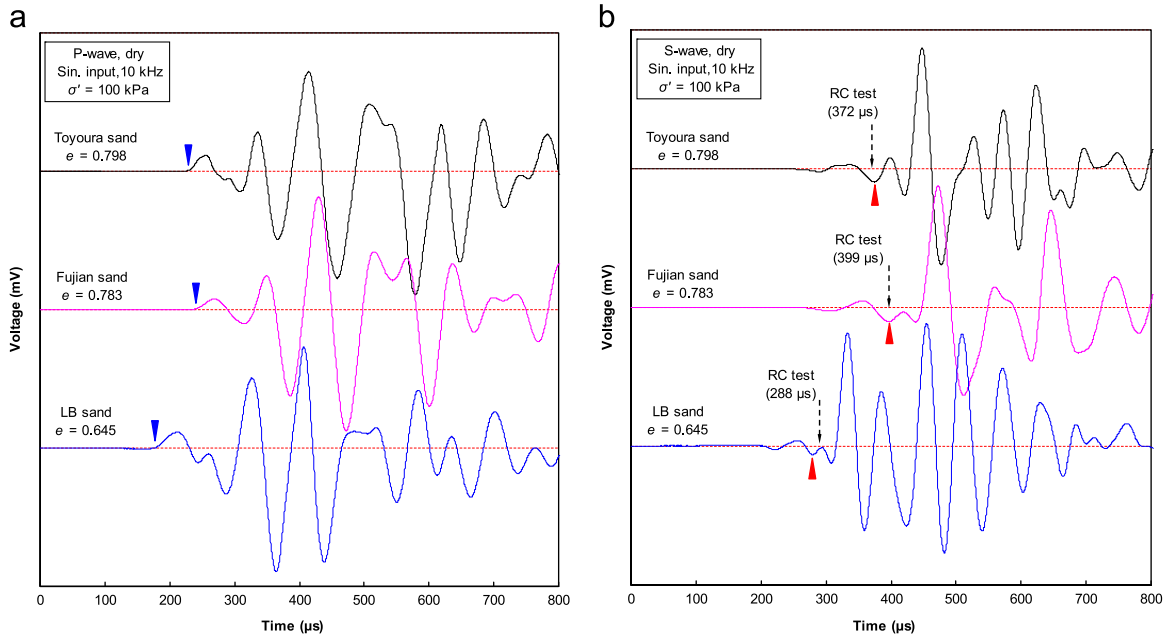

Fig. 7. Comparison of received signals in three sands: (a) P-wave; and (b) S-wave.

as the coefficient of uniformity of sand increases (Wichtmann and Triantafyllidis, 2010).

Currently there are two major explanations for the discrepancy in the n values between the experimental data and the theoretical prediction. The first possible explanation attributes the discrepancy to the difference between the Hertz–Mindlin contact law and the actual contact condition, thus leading to several modified contact laws. For example, Goddard (1990) proposed a contact law for conical contacts of which stress exponent n changes from 1/2 to 1/3 when the confining pressure exceeds a transition value. However, there is experimental evidence that values for n, for assemblies of spherical steel balls and glass beads, are similar to those for angular sands (Duffy and Mindlin, 1957; Yang and Gu, 2013).

The second possible explanation attributes the discrepancy to the change in fabric (e.g., contact number) during the increase in confining pressure that causes an additional increase in stiffness (McDowell and Bolton, 2001). In the experiments of Duffy and Mindlin (1957) on the face-centered cubic packing of two types of steel spheres (i.e., low and high tolerance spheres), the measured n values are higher than the value of 1/3 of those predicted by the Hertz contact, especially for the low tolerance spheres. Duffy and Mindlin (1957) speculated that the discrepancy was probably due to the evolution of contacts between the steel spheres. The discrete element simulations of Gu (2012) corroborate this assumption. Therefore, the n value should increase with an increasing void ratio as the evolution of the fabric is expected to be more significant in the loose specimen. In order to check this assumption, the stress exponent n of each specimen is plotted against its initial void ratio in Fig. 10. Evidently, the n value for G_0 increases with an increasing void ratio, as expected. However, the n value for M_0 tends to decrease as the void ratio increases, which contradicts the assumption. For each of the three sands, the average stress exponent n for G_0 is

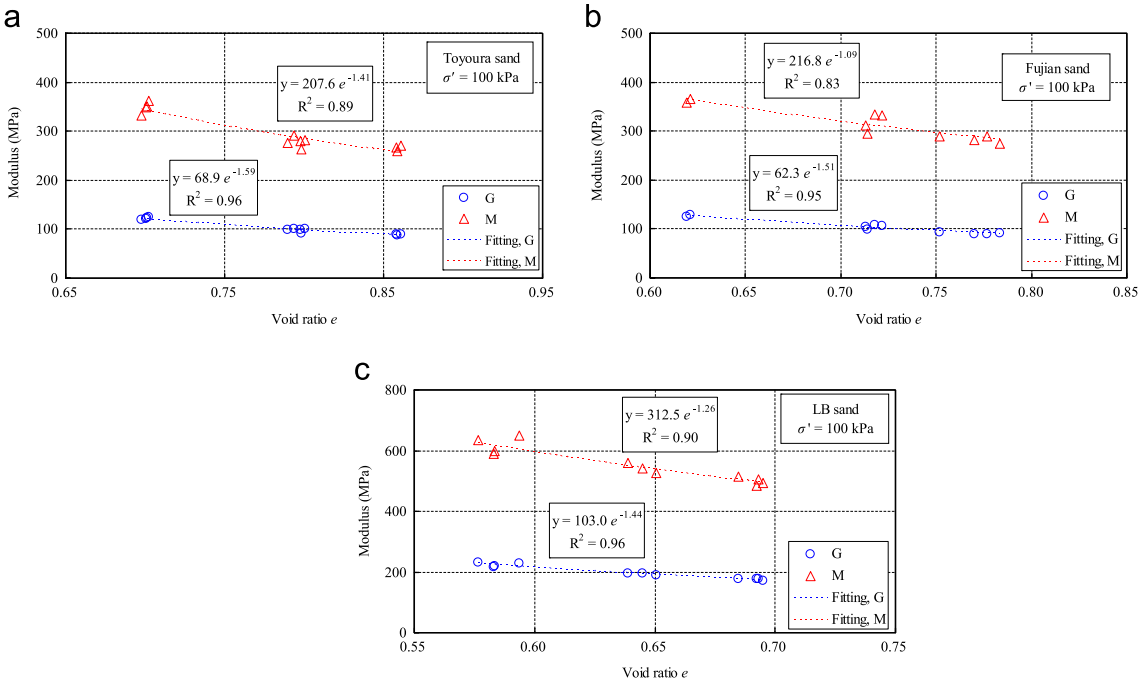

Fig. 8. Variation of G_0 and M_0 with void ratio for (a) Toyoura, (b) Fujian and (c) LB sands.

Table 2
Values of exponent x in void ratio function for different properties.

σ' (kPa)	Toyoura sand			Fujian sand			LB sand		
	G_0	M_0	υ	G_0	M_0	υ	G_0	M_0	υ
50	1.65	1.37	−0.39	1.60	1.12	−0.62	1.46	1.20	−0.47
100	1.59	1.41	−0.30	1.51	1.09	−0.64	1.44	1.26	−0.35
200	1.58	1.46	−0.21	1.50	1.20	−0.51	1.44	1.14	−0.62
400	1.48	1.35	−0.26	1.45	1.22	−0.46	1.39	1.20	−0.43
Average	1.57	1.40	−0.29	1.51	1.16	−0.56	1.44	1.20	−0.47

always larger than that for M_0 (difference around 0.03–0.05). Hence, G_0 will increase faster than M_0 as the confining pressure increases, resulting in a decrease in Poisson's ratio with increasing pressure.

For comparison purposes, the G_0 and M_0 of the three tested sands are normalized by the commonly used void ratio function $F(e)=(2.17-e)^2/(1+e)$ and plotted as a function of the normalized confining pressure in Fig. 11. The values of normalized G_0 and M_0 of Toyoura sand are around 10% larger than those of Fujian sand. Both the G_0 and M_0 values of Fujian and Toyoura sands are significantly smaller (40–60%) than those of LB sand. Hoque and Tatsuoka (1998) also observed that the axial Young's modulus of LB sand is much larger than that of other clean uniform sands and gravels at identical confining pressures and void ratios. It seems that such a difference is not induced by their gradation, as they have similar values for coefficients of uniformity and the mean particle size has an ignorable effect on the elastic modulus (Iwasaki and Tatsuoka, 1977; Wichtmann and Triantafyllidis, 2010; Yang and Gu, 2013). Iwasaki and Tatsuoka (1977) also indicated that the difference in the normalized G_0 values of various clean sands with different particle shapes is generally less than 10%, which means that the difference observed in the present study should not be primarily due to the difference in the particle shapes of the tested sands. A possible reason could be the difference in individual particle contact stiffness due to difference in the mineralogy or the surface roughness of the grains. For example, Santamarina and Cascante (1998) measured the wave velocity in mildly rusted and rusted steel spheres and indicated that the surface roughness may significantly decrease the stiffness. The discrepancy in the n values, between the experimental data and the theoretical prediction by the Hertz–Mindlin contact, is probably due to the combination of both effects, namely, contact shape and fabric evolution.

3.3. Poisson's ratio υ and its relation to G_0 and M_0

Poisson's ratio at each tested combination of void ratio and confining pressure is evaluated based on the measured V_s and V_p. Fig. 12 shows the relation between Poisson's ratio and the void ratio at confining pressures of 100 kPa and 400 kPa. Evidently, at a given pressure, Poisson's ratio increases as the void ratio increases, although some scatter exists. Meanwhile, at the same void ratio, Poisson's ratio decreases as the confining pressure increases. Similar to the elastic modulus, the void ratio function, $F(e)=e^{-x}$, is also used to characterize the effect of the void ratio on Poison's ratio. The best-fit parameters at each confining pressure are listed in Table 2. To quantitatively describe the effect of the confining pressure on Poisson's ratio, the normalized Poisson's ratio, $\upsilon/F(e)$, is fitted by a power law relationship, as shown in Fig. 13. The stress exponent is −0.09 for both Toyoura sand and Fujian sand, while it is −0.05 for LB sand. The functions describing the pressure and the density dependence of Poisson's ratio are given in Fig. 13. The above results indicate that Poisson's ratio for a

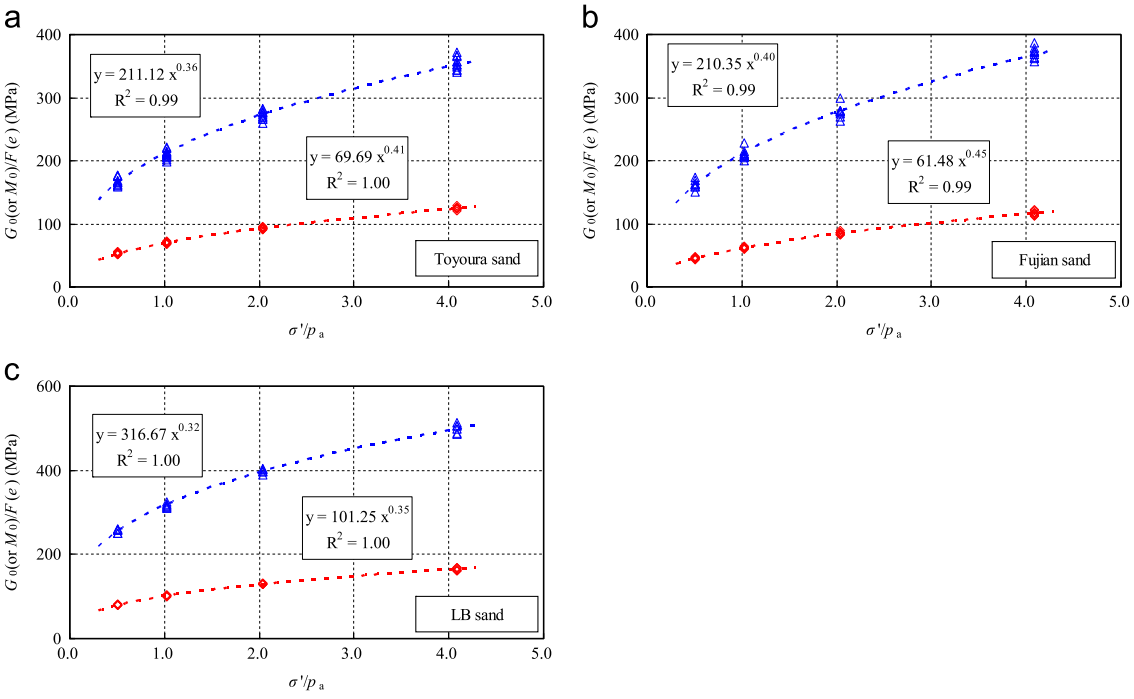

Fig. 9. Relation between normalized modulus and pressure for (a) Toyoura, (b) Fujian and (c) LB sands.

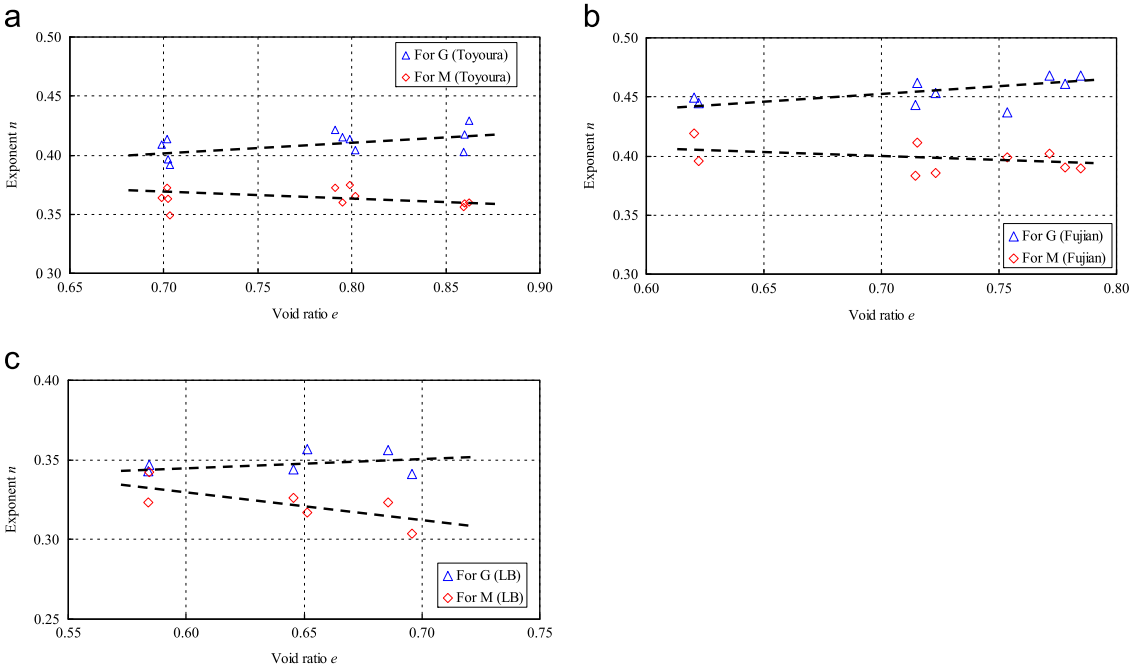

Fig. 10. Variation of stress exponent n with initial void ratio for (a) Toyoura, (b) Fujian and (c) LB sands.

granular material is not a constant, but decreases with a decreasing void ratio and an increasing confining pressure.

Bearing in mind that G_0, M_0 and υ all depend on the void ratio and confining pressure, it is possible to establish correlations between υ and G_0 or M_0. It is meaningful to establish such correlations since G_0 and M_0 are usually not measured simultaneously in the laboratory or field. Fig. 14 plots υ against G_0 or M_0. The data from the present study is shown together with the data on clean sands in the literature. Generally, υ is in the range of 0.15–0.33 for the range of G_0 and M_0 considered in Fig. 14. υ tends to decrease with an increasing G_0 and M_0, especially at low values of G_0 and M_0. Such a trend is expected because υ decreases, but G_0 and M_0 increase with a decreasing void ratio and an increasing confining pressure. It is encouraging to note that, to some extent, the relation between υ and G_0 (or M_0) is unique for different sands, although the data is

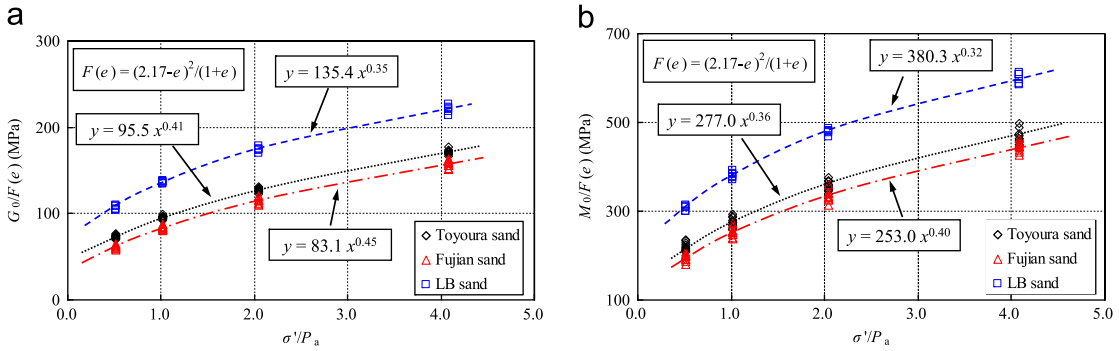

Fig. 11. Relation between normalized modulus and pressure for (a) G_0 and (b) M_0.

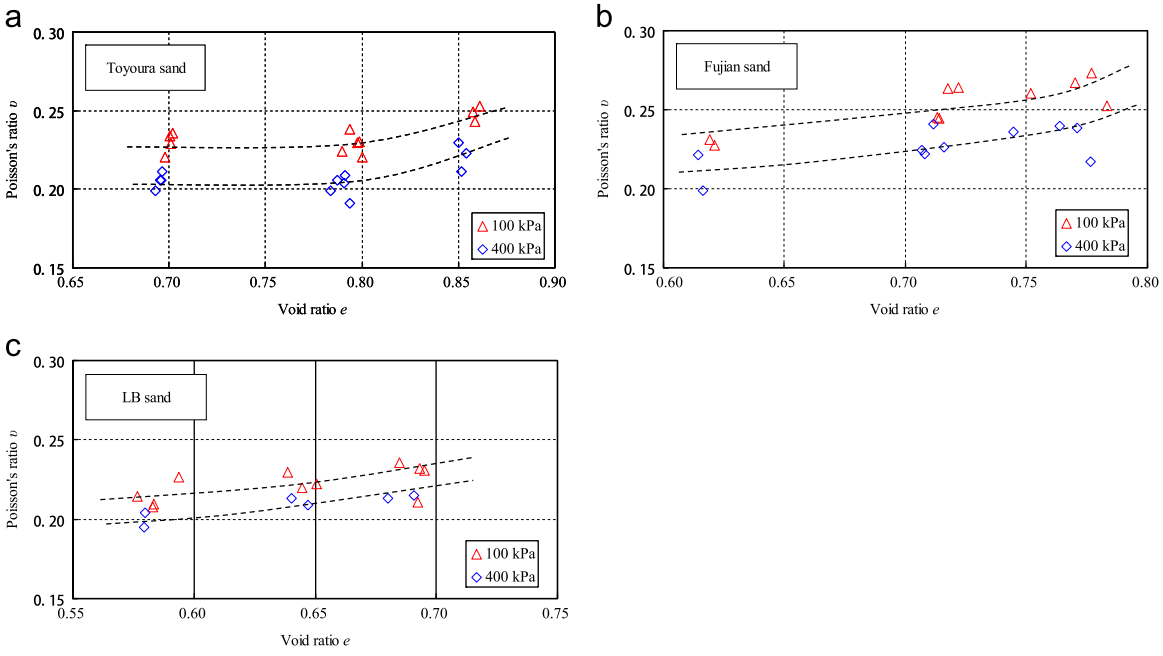

Fig. 12. Variation of Poisson's ratio with void ratio for (a) Toyoura, (b) Fujian and (c) LB sands.

somewhat scattered. Empirical equations with a power law are used to quantitatively link υ and G_0 or M_0, as follows:

$$\upsilon = 0.620(G_0)^{-0.200} \tag{6}$$

and

$$\upsilon = 0.846(M_0)^{-0.216} \tag{7}$$

Therefore, Poisson's ratio for dry granular soil may be approximately estimated from the measured G_0 or M_0, using Eqs. (6) and (7).

4. Summary and conclusions

The S-wave and P-wave velocities in three dry sands at various densities and confining pressures were simultaneously measured by a single pair of bender elements incorporated in a standard resonant column (RC) apparatus with a torsional shear (TS) function. The effect of the void ratio and the confining pressure on the small strain properties, including shear modulus G_0, constrained modulus M_0 and Poisson's ratio υ, was investigated. The major findings in the paper can be summarized as follows:

(a) It is easy to determine the first arrival in the P-wave test, but difficult in the S-wave test primarily due to the near field effect. Meanwhile, the first arrivals of both the P-wave and the S-wave are generally smaller in amplitude than the succeeding ones. The consistency of the G_0 values for Toyoura sand obtained from BE, RC and TS tests in this study, as well as the good agreement with the data in the literature, illustrates the reliability of the signal interpretation and the testing system.

(b) For each of the three sands, the void ratio and the pressure dependence was found to be larger for G_0 than for M_0. The average stress exponents n in the empirical equation for both G_0 and M_0 are generally larger than 1/3 for the Hertz–Mindlin contact law. Stress exponent n for G_0 tends to increase with an increasing void ratio, while for M_0 the opposite trend is observed.

(c) The normalized G_0 and M_0 values of Toyoura sand are around 10% higher than those of Fujian sand, and significantly lower (40–60%) than those of LB sand. A possible reason could be the difference in individual particle contact stiffness due to the different particle surface properties (e.g.,

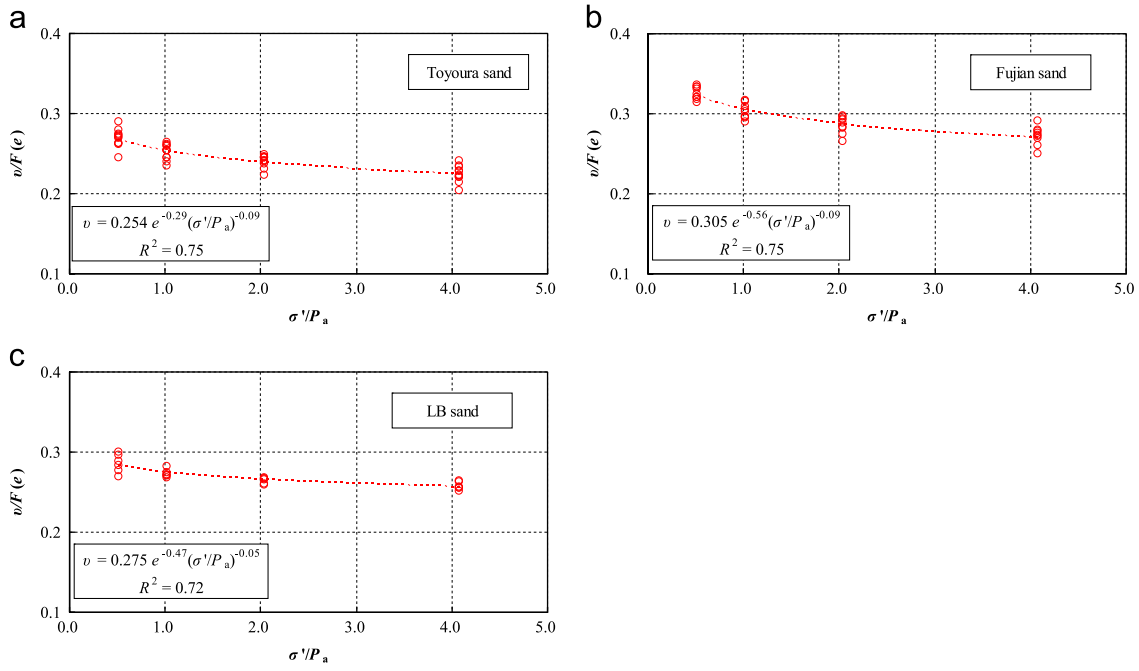

Fig. 13. Variation of Poisson's ratio with pressure for (a) Toyoura, (b) Fujian and (c) LB sands.

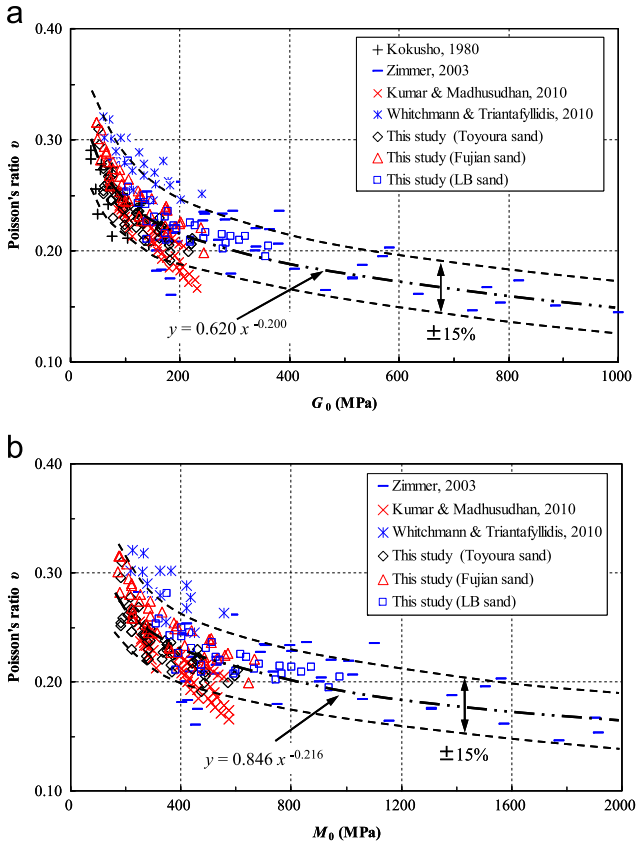

Fig. 14. Variation of Poisson's ratio with (a) G_0 and (b) M_0 (Zimmer, 2003).

surface roughness). Further research is needed to clarify this issue.

(d) Poisson's ratio υ decreases as the void ratio decreases and the confining pressure increases. Poisson's ratio of the three tested sands is generally in the range of 0.18–0.32 at various void ratios and confining pressures. Empirical equations are established to approximately estimate Poisson's ratio from the measured G_0 or M_0 values.

Acknowledgments

The work presented in this paper was supported by the Seed Funding for Basic Research Scheme (Grant no. 201011159098) from The University of Hong Kong and the National Basic Research Program of China (973 Program, Grant no. 2012CB719803). Their support is gratefully acknowledged. The authors are also very thankful to the reviewers for their valuable comments and suggestions.

References

Andrus, R.D., Stokoe, K.H. II., 2000. Liquefaction resistance of soils from shear-wave velocity. Journal of Geotechnical and Geoenvironmental Engineering 126 (11), 1015–1025.

Bonal, J., Donohue, S., McNally, C., 2012. Wavelet analysis of bender element signals. Géotechnique 62 (3), 243–252.

Brignoli, E.G.M., Gotti, M., Stokoe, K.H. II., 1996. Measurement of shear waves in laboratory specimens by means of piezoelectric transducers. Geotechnical Testing Journal 19 (4), 384–397.

Cascante, G., Santamarina, C., Yassir, N., 1998. Flexural excitation in a standard torsional resonant column device. Canadian Geotechnical Journal 35, 478–490.

Chaudhary, S.K., Kuwano, J., Hayano, Y., 2003. Measurement of quasi-elastic stiffness parameters of dense Toyoura sand in hollow cylinder apparatus and triaxial apparatus with bender elements. Geotechnical Testing Journal 27 (1), 23–35.

Duffy, J., Mindlin, R.D., 1957. Stress–strain relations and vibrations of a granular medium. Journal of Applied Mechanics 24, 585–593.

Dyvik, R., Madshus, C., 1985. Lab measurements of G_{max} using bender element. In: Khosla, V. (Ed.), Advances in the Art of Testing Soils under Cyclic Conditions. ASCE, New York, pp. 186–196.

Ezaoui, A., Di Benedetto, H., 2009. Experimental measurements of the global anisotropic elastic behavior of dry Hostun sand during triaxial tests, and the effect of sample preparation. Géotechnique 59 (7), 621–635.

Goddard, J.D., 1990. Nonlinear elasticity and pressure-dependent wave speeds in granular media. Proceedings of the Royal Society of London A 430, 105–131.

Gu, X.Q., 2012. Dynamic properties of granular materials at the macro and micro scales (Ph.D. Thesis), The University of Hong Kong, Hong Kong.

Hardin, B.O., Richart, F.E., 1963. Elastic wave velocities in granular soils. Journal of The Soil Mechanics and Foundations Division 89 (SM1), 39–56.

Hoque, E., Tatsuoka, F., 1998. Anisotropy in elastic deformation of granular materials. Soils and Foundations 38 (11), 163–179.

Iwasaki, T., Tatsuoka, F., 1977. Effect of grain size and grading on dynamic shear moduli of sand. Soils and Foundations 17 (3), 19–35.

Kokusho, T., 1980. Cyclic triaxial test of dynamic soil properties for wide strain range. Soils and Foundations 20 (2), 45–60.

Kumar, J., Madhusudhan, B.N., 2010. Effect of relative density and confining pressure on Poisson ratio from bender–extender element tests. Géotechnique 60 (7), 561–567.

Lee, J.-S., Santamarina, J.C., 2005. Bender element, performance and signal interpretation. Journal of Geotechnical and Geoenvironmental Engineering 131 (9), 1063–1070.

Leong, E.C., Cahyadi, J., Rahardjo, H., 2009. Measuring shear and compression wave velocities of soil using bender–extender elements. Canadian Geotechnical Journal 46, 792–812.

Lings, M.L., Greening, P.D., 2001. A novel bender/extender element for soil testing. Géotechnique 51 (8), 713–717.

Lo Presti, D.C.F., Jamiolkowski, M., Pallara, O., Cavallaro, A., Pedroni, S., 1997. Shear modulus and damping of soils. Géotechnique 47 (3), 603–617.

McDowell, G.R., Bolton, M.D., 2001. Micro mechanics of elastic soil. Soils and Foundations 41 (6), 147–152.

Murillo, C., Sharifipour, M., Caicedo, B., Thorel, L., Dano, C., 2011. Elastic parameters of intermediate soils based on bender–extender elements pulse tests. Soils and Foundations 51 (4), 637–649.

Nakagawa, K., Soga, K., Mitchell, J.K., 1997. Observation of Biot compressional wave of the second kind in granular soils. Géotechnique 47 (1), 133–147.

Richart, F.E., Hall, J.R., Woods, R.D., 1970. Vibrations of Soils and Foundations. Prentice-Hall, Englewood Cliffs, New Jersey.

Sanchez-Salinero, I., Roesset, J.M., Stokoe, K.H. II., 1986. Analytical Studies of Body Wave Propagation and Attenuation. Report no. GR-86-15. University of Texas, Austin, Texas.

Santamarina, J.C., Cascante, G., 1998. Effect of surface roughness on the wave propagation parameters. Géotechnique 48 (1), 129–136.

Tatsuoka, F., Iwasaki, T., Yoshida, S., Fukushima, S., Sudo, H., 1979. Shear modulus and damping by drained tests on clean sand specimens reconstituted by various methods. Soils and Foundations 19 (1), 39–54.

Viggiani, G., Atkinson, J.H., 1995. Interpretation of bender element tests. Géotechnique 45 (1), 149–154.

Wang, Y.H., Lo, K.F., Yan, W.M., Dong, X.B., 2007. Measurement biases in the bender element test. Journal of Geotechnical and Geoenvironmental Engineering 133 (5), 564–574.

Wichtmann, T., Triantafyllidis, T., 2010. On the influence of the grain size distribution curve on P-wave velocity, constrained elastic modulus M_{max} and Poisson's ratio of quartz sands. Soil Dynamics and Earthquake Engineering 30 (8), 757–766.

Yamashita, S., Kawaguchi, T., Nakata, Y., Mikami, T., Fujiwara, T., Shibuya, S., 2009. Interpretation of international parallel test on the measurement of G_{max} using bender elements. Soils and Foundations 49 (4), 631–650.

Yang, J., Gu, X.Q., 2013. Shear stiffness of granular material at small strain: does it depend on grain size? Géotechnique 63 (2), 165–179.

Yang, J., Yan, X.R., 2009. Site response to multi-directional earthquake loading: a practical procedure. Soil Dynamics and Earthquake Engineering 29 (4), 710–721.

Youn, J.-U., Choo, Y.-W., Kim, D.-S., 2008. Measurement of small-strain shear modulus G_{max} of dry and saturated sands by bender element, resonant column, and torsional shear tests. Canadian Geotechnical Journal 45, 1426–1438.

Zimmer, M.A., 2003. Seismic velocities in unconsolidated sands: measurements of pressure, sorting and compaction effects (Ph.D. Thesis), Stanford University, USA.